Applied Surface Science 256 (2009) 423–427

Contents lists available at ScienceDirect

Applied Surface Science

journal homepage: www.elsevier.com/locate/apsusc

Hierarchical nanoparticle morphology for platinum supported on $SrTiO_3$ (0 0 1): A combined microscopy and X-ray scattering study

Steven T. Christensen [a], Byeongdu Lee [b], Zhenxing Feng [a], Mark C. Hersam [a,c], Michael J. Bedzyk [a,d,e,*]

[a] Department of Materials Science and Engineering, Northwestern University, Evanston, IL 60208, USA
[b] X-ray Science Division, Advanced Photon Source, Argonne National Laboratory, Argonne, IL 60439, USA
[c] Department of Chemistry, Northwestern University, Evanston, IL 60208, USA
[d] Materials Science Division, Argonne National Laboratory, Argonne, IL 60439, USA
[e] Department of Physics and Astronomy, Northwestern University, Evanston, IL 60208, USA

ARTICLE INFO

Article history:
Available online 11 June 2009

Keywords:
Nanoparticles
Platinum
$SrTiO_3$
AFM
GISAXS
SEM

ABSTRACT

The morphology of metal nanoparticles supported on oxide substrates plays an important role in heterogeneous catalysis and in the nucleation of thin films. For platinum evaporated onto $SrTiO_3$ (0 0 1) and vacuum annealed we find an unexpected growth formation of Pt nanoparticles that aggregate into clusters without coalescence. This hierarchical nanoparticle morphology with an enhanced surface-to-volume ratio for Pt is analyzed by grazing incidence small-angle X-ray scattering (GISAXS), X-ray fluorescence (XRF), atomic force microscopy (AFM) and high-resolution scanning electron microscopy (SEM). The nanoparticle constituents of the clusters measure 2–4 nm in size and are nearly contiguously spaced where the average edge-to-edge spacing is less than 1 nm. These particles make up the clusters, which are 10–50 nm in diameter and are spaced on the order of 100 nm apart.

1. Introduction

For interfacial applications such as chemical sensing and catalysis, maximizing the surface area-to-volume ratio of the active species can ensure high chemical activity. Suppressing deleterious losses in surface area through coalescence and sintering mechanisms remains a key challenge. Furthermore, creating well-dispersed nanoparticles with a high-surface area is vital to the economic viability of many catalyst architectures that employ noble metals such as platinum. Platinum nanoparticles (1–3 nm in size) have recently shown an intriguing behavior to aggregate without coalescence or sintering into clusters ranging from 10 to 50 nm across [1,2]. Similar structures were observed with FePt cluster deposition [3] whereas gold and indium cluster deposition resulted in coalescence [1,2]. Such hierarchical nanostructures appear to defy thermodynamic driving forces and maintain long-term stability [2]. Using complementary high-resolution microscopy and X-ray techniques, we report on the formation of nanoparticle morphology for platinum on $SrTiO_3$ (0 0 1) that possesses a similar structure where small Pt nanoparticles have aggregated into clusters without complete coalescence. Although platinum is the common ingredient to these aggregate-based structures, the morphology observed herein resulted from annealing ultra-thin platinum films evaporated onto $SrTiO_3$ (0 0 1) substrates. The Pt/$SrTiO_3$ system serves as a model photocatalyst system that can be employed to induce hydrolysis for hydrogen production [4,5]. Photocatalytic performance was directly correlated to ultra-thin Pt films on $SrTiO_3$, which presumably consisted of Pt nanoparticles but at that time were not detectable with nondestructive methods [6]. This material performance offers additional motivation for developing hierarchical Pt nanostructures, which have a high-surface area and are resistant to coalescence.

In addition to identifying another class of aggregate-based platinum nanoparticle morphology, this report employs a multi-length scale characterization methodology that offers flexibility for quantifying the size and spacing of the nanoclusters and their constituents. In the previous reports for cluster deposition, the key dimensions were successfully obtained with transmission electron microscopy (TEM) [1–3]. Our method employs a combination of atomic force microscopy [7] (AFM) and grazing incidence small-angle X-ray scattering [8] (GISAXS) to enable direct observation and characterization of supported nanoparticles. Surprisingly, AFM and GISAXS are not often paired together despite the fact that the two techniques provide a very useful means for quantifying the structural properties of supported

* Corresponding author at: Department of Materials Science and Engineering, Northwestern University, 2220 Campus Dr., Evanston, IL 60208, USA.
Tel.: +1 847 491 3570; fax: +1 847 491 7820.
E-mail address: bedzyk@northwestern.edu (M.J. Bedzyk).

0169-4332/$ – see front matter © 2009 Elsevier B.V. All rights reserved.
doi:10.1016/j.apsusc.2009.06.017

nanoparticles [9,10]. GISAXS analysis accesses length scales below the resolution-limit of AFM, while AFM evaluates length scales above the GISAXS upper limit. Our initial GISAXS and AFM analysis indicated the Pt nanoparticles were clustering without total coalescence. These results were independently confirmed using high-resolution scanning electron microscopy (SEM). The characterization of these hierarchical nanostructures is an important first step in their development as it shows that structures of this nature are not necessarily confined to specific support materials and geometries.

2. Materials and methods

Substrate preparation. $SrTiO_3$ (0 0 1) substrates (10 mm × 10 mm × 1 mm, MTI Corp.) were ultrasonically cleaned for 5 min in acetone, isopropanol, and deionized water (18 MΩ/cm) for 15 min. The substrates were then etched in a hydrofluoric acid/ammonium fluoride solution (Riddel-de Haen part no. 40207; pH ∼ 5) for approximately 45 s, and then the substrates were rinsed in deionized water and dried with N_2. After etching, the substrates were loaded into a tube furnace with flowing O_2 (∼100 sccm) and annealed at 1050 °C for 5 h. This treatment produces atomically flat terraces terminated with titanium oxide [11,12]. After annealing in oxygen, the substrates were immediately mounted on a tantalum sample plate using spot-welded tantalum wire and loaded into a high-vacuum chamber. The vacuum chamber was maintained at a pressure between 10^{-9} and 10^{-10} Torr and equipped with low-energy electron diffraction (LEED; Omicron), Auger electron spectroscopy (Physical Electronics), and an electron beam effusion source (Omicron). Prior to platinum deposition, the substrates were annealed at 925 °C for 30 min in the vacuum chamber using an indirect tungsten wire heater placed behind the sample. LEED measurements before and after annealing indicated the presence of the $\sqrt{13} \times \sqrt{13}$ R33.7° surface reconstruction [13], and Auger electron spectroscopy revealed a reduction of the carbon peak to an undetectable level after annealing. Platinum electron beam deposition of a 1.5 mm diameter Pt rod occurred in a side chamber pumped by a turbomolecular pump where the pressure did not exceed 10^{-9} Torr. The platinum source to sample distance was 80 mm and the platinum temperature at deposition was measured to be approximately 1750 °C. Platinum was deposited for 10 min, which was followed by a 10 min post-deposition anneal at 900 °C.

Imaging. AFM measurements were performed in air using a Thermomicroscopes CP Research AFM operated in intermittent contact mode. Silicon AFM tips (μMasch) with a nominal 10 nm radius of curvature and cantilever resonant frequency of ∼70 kHz were used. Image analysis included polynomial subtraction to correct for curvature in the image resulting from piezo tube motion. AFM heights were calibrated using the 0.39 nm atomic steps of $SrTiO_3$ (0 0 1) and the 0.32 nm steps of TiO_2 (1 1 0). SEM images were collected on the imaging column of a FEI Helios system, which employs a field emission gun. The samples were imaged without any additional treatment to improve conductivity (e.g. gold coating).

X-ray measurements. GISAXS measurements were performed at the Advanced Photon Source (APS) 12ID-C beam line. Scattered X-rays were collected on a 2048 × 2048 CCD detector (MAR) after passing through an evacuated flight path with a detector-to-sample distance of 1 m for E_γ = 11.50 keV and 2.1 m for E_γ = 8.00 keV. The scattering is given in terms of the scattering vector or momentum transfer vector $\mathbf{q} = \mathbf{k_f} - \mathbf{k_i}$, where $\mathbf{k_i}$ and $\mathbf{k_f}$ are the incident and scattered wave vectors, respectively. It is convenient to use the Cartesian components (q_x, q_y, q_z) of the momentum transfer where the vertical dimension (height) of supported nanostructures is related to out-of-plane component (q_z) and the lateral dimension and spacing is related to the in-plane component: $q_{xy} = \sqrt{q_x^2 + q_y^2}$ [14]. GISAXS data were calibrated using a silver behenate standard, and images were corrected for detector dark counts. X-ray fluorescence data (XRF) were collected at the APS 5ID-C station using an energy-dispersive silicon drift diode detector (Vortex, SII NanoTechnology) at an incident photon energy of 15.00 keV. The platinum coverage was determined through a comparison of the Pt Lα (9.40 keV) X-ray fluorescence yield to a standard with a calibrated Pt coverage.

3. Results

The XRF measured platinum total coverage is $\Theta_T = 0.93 \pm 0.05$ ML (monolayers), where 1 ML = 6.558 nm^{-2}, which corresponds to the 2D atomic density of Sr or Ti in a (0 0 1) plane of cubic-P $SrTiO_3$ with lattice constant a_{STO} = 0.3905 nm. Fig. 1(a) shows a typical AFM image of the Pt nanoclusters after preparation where they decorate the surface with no particular order. The AFM was performed in tapping mode and confirmed to have no significant manipulation of the nanoclusters. The images also show features related to the atomic steps of the $SrTiO_3$, which can be used to calibrate height measurements on an image-by-image basis. Analysis of several AFM images yields an average nanoparticle height of 4.6 nm with a distribution width of 1.2 nm, which is represented by the histogram in Fig. 1(b). The average interparticle spacing from AFM was 85 nm.

Fig. 2 shows the GISAXS data from the CCD detector collected at two different conditions representing a course and a fine length scale. For Fig. 2(a) (E_γ = 8.00 keV) the GISAXS conditions emphasize larger structures and analysis of horizontal line sections in q_{xy} of the CCD image enables the determination of the lateral dimension (R_g) of the nanoclusters by way of the Guinier approximation [15], which is based on the following expression for the scattered intensity, $I(q_{xy})$:

$$I(q_{xy}) \propto \exp\left(-\frac{1}{3}R_g^2 q_{xy}^2\right). \quad (1)$$

Guinier analysis, Fig. 2(c), thus yields an average lateral nanoparticle dimension of R_g = 18 nm, which is in agreement with the AFM image of Fig. 1, taking into account the AFM tip convolution. Fig. 2(a) also shows a scattering feature at higher q_{xy} that is more pronounced by the GISAXS data shown in Fig. 2(b). It consists of an intensity lobe with a peak shaped feature that is related to the pair distribution of nanostructures spaced on a finer

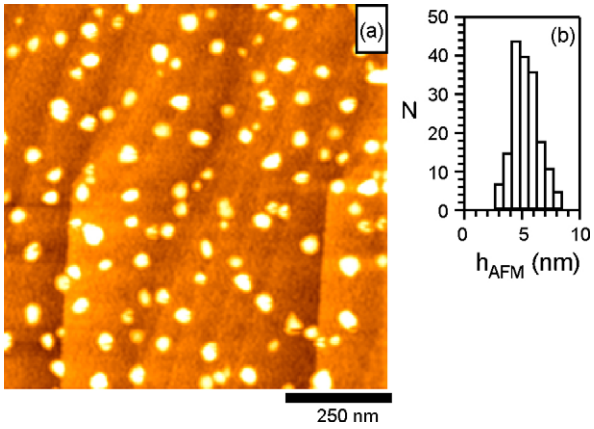

Fig. 1. AFM data. (a) Typical AFM image showing nanoparticles and the $SrTiO_3$ (0 0 1) atomic terraces. (b) Histogram of the height measurements from several AFM images. The average height of the nanoparticles from AFM is 4.6 nm with a distribution width of 1.2 nm.

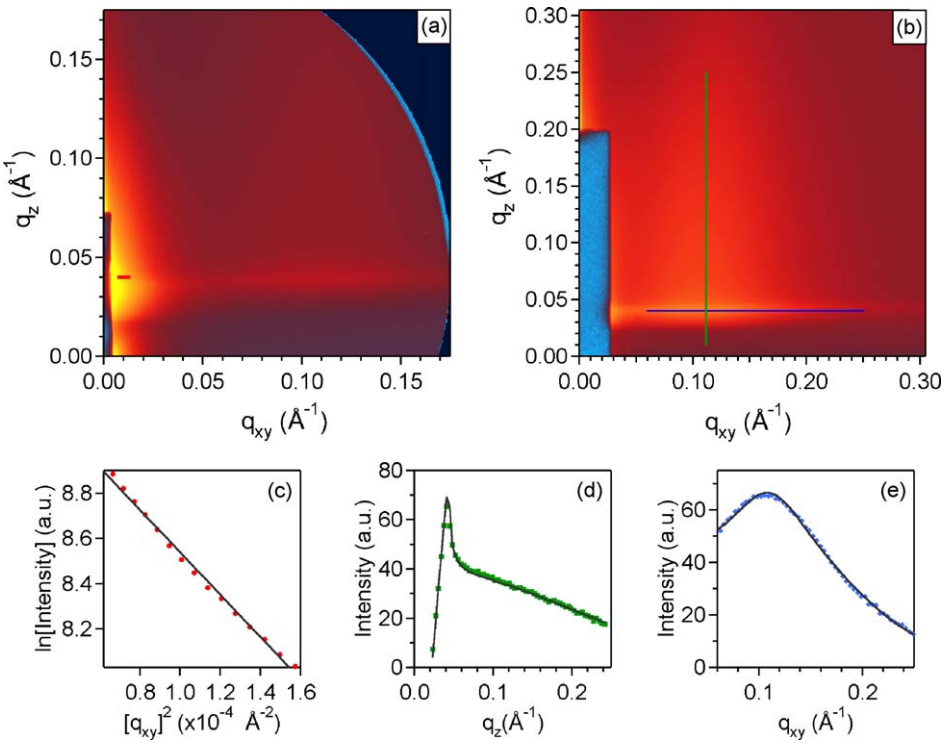

Fig. 2. GISAXS data, where q_{xy} and q_z are the in-plane and out-of-plane components of the scattering vector, respectively. (a) CCD data taken at E_γ = 8.00 keV to emphasize nanoparticle sizes similar to the nanoparticles in the AFM data shown in Fig. 1. The data also show scattered intensity in the region of $q_{xy} \sim 0.1$ Å^{-1} that is related to lateral features smaller than the resolution of the AFM tip. (b) CCD data taken at E_γ = 11.50 keV that emphasizes the finer length scale near the $q_{xy} \sim 0.1$ Å^{-1} region. (c) Guinier plot of a lateral line cut at q_z = 0.04 Å^{-1} from (a) where the slope of this line gives the average lateral nanoparticle dimension of 18 nm. (d) Vertical line cut at q_{xy} = 0.11 Å^{-1} and fit that gives the average nanoparticle height from GISAXS to be 1.8 nm. (e) Horizontal line cut at q_z = 0.04 Å^{-1} and fit which gives a lateral dimension of 1.9 nm and center-to-center spacing of 4.2 nm. The combined GISAXS analysis suggests that the platinum nanoparticles have a hierarchical structure where smaller nanoparticles have aggregated into clusters without complete coalescence.

scale than those observed with AFM. The horizontal and vertical line cuts, Fig. 2(d and e), from the CCD data of this region were fit using the IsGISAXS program [14] that incorporated a theory framework including the distorted-wave Born approximation [14,16–19] for a cylinder form factor and the local monodisperse approximation [20] with 1D paracrystal model [14,21]. The fitting results indicated that on this finer scale the lateral dimension, height, and the center-to-center interparticle spacing are: R_P = 1.8 nm, h_P = 1.9 nm, and D = 4.2 nm, respectively. The GISAXS height measurement is an ensemble average of the vertical dimensions whereas the AFM height measurement measures the tallest particle in a cluster. These dimensions and spacing would suggest that in the lateral direction the nanoparticles are nearly touching. If this were a contiguous film of particles it would constitute several monolayers of Pt, which would contradict the XRF determined coverage. The uncertainties are ~10% for the fitted values from both the Gunier and GISAXS analysis.

In addition to collecting AFM and GISAXS data, we were able to obtain high-resolution SEM images of the Pt nanoparticles without the use of an additional conductive coating or treatment to enhance the imaging properties. The SEM image in Fig. 3 shows features that support the AFM and GISAXS results. Namely, nanoparticles are observed with a lateral dimension between 10 and 50 nm that are spaced ~100 nm apart as is the case with the AFM data. These particles appear to consist of smaller nanoparticles a few nanometers in size. The constituent nanoparticles are comparable to the smallest nanoparticle dimensions detected by GISAXS. In addition to the large nanoparticles, there are features related to the atomic terraces observed in AFM. The SEM image also shows a granular texture in between the nanoparticles. We conclude that the texture does not contain a significant (measurable) fraction of the total Pt coverage, since the GISAXS data does not indicate a multi-modal size distribution of individual Pt nanoparticles and the XRF measured 1 ML Pt coverage can be accounted for by the volume of the larger clusters as estimated from AFM and GISAXS. The texture is most likely related to carbon deposition from the SEM

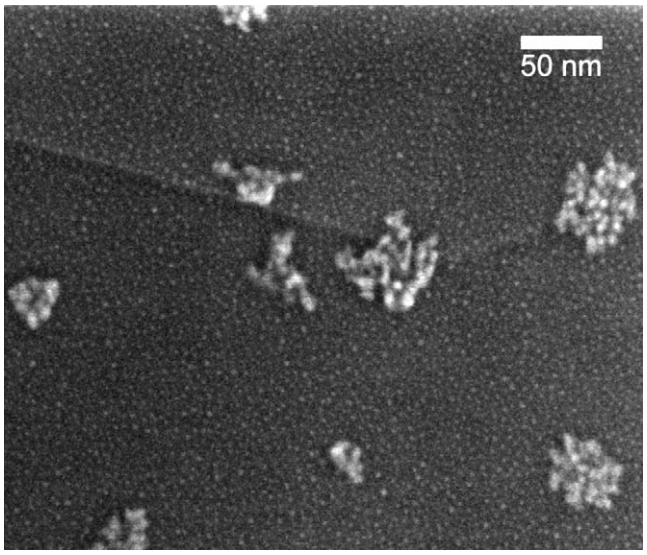

Fig. 3. High-resolution SEM image showing Pt nanoclusters. The size and spacing of the clusters and their constituent nanoparticles agrees with the combined AFM and GISAXS analysis. The image also shows the features due to atomic terraces.

probe. The image was collected at an operating voltage of 3 kV and 21 pA.

4. Discussion

Prior to obtaining the SEM images, the AFM and GISAXS results were interpreted to suggest that platinum nanoparticles have aggregated without coalescence or sintering to form nanoparticle clusters. The addition of the SEM confirms the presence of nanoparticle clusters; the large nanoparticles appear to be hierarchal structures with an overall lateral dimension in agreement with the Guinier analysis and AFM. The dimensions of the components of the nanoclusters from SEM agree with the GISAXS fitting of the data collected at the finer scale. The formation of Pt nanoparticles that do not completely coalesce to minimize the platinum surface area is a somewhat unexpected result. The driving forces to minimize surface area normally would lead to growth and coarsening mechanisms that would broaden the size distribution as nanoparticles sinter and coalesce.

Supported platinum nanoparticles have recently been observed to display a resistance to such processes [1–3]. Using cluster beam deposition sources, ~2 nm platinum nanoparticles have been deposited on various carbon supports at room temperature. TEM images show that the nanoparticles aggregate into clusters where the nanoparticles are spaced closely but not touching and do not further sinter or coalesce. These studies compared the Pt behavior to other elements such as gold and indium, both of which underwent some form of sintering and coalescence. The mechanism attributed to the cluster deposited nanoparticles resisting complete coalescence involves the buckling of the carbon support to create a diffusion barrier to the Pt species [2]. Alternative mechanisms that may kinetically hinder thermodynamic forces could be manifested through the chemical state of the Pt or a physical barrier.

One possibility behind the formation of nanoparticle clusters that do not completely sinter is related to both the Pt chemical state and a physical barrier. Bulk metallic platinum is well known to resist oxidation, but platinum nanoparticle properties are likely to deviate from the bulk. The formation of platinum oxide nanostructures on $SrTiO_3$ (0 0 1) surfaces through thermal processing is not surprising. Several related systems containing platinum or palladium supported on TiO_2 and $SrTiO_3$ have been shown to form encapsulating TiO_x layers around the metal nanoparticles upon annealing in vacuum [22–24]. The annealing conditions we employ are thus likely to induce some significant changes in the make-up of the platinum on the surface. However, it is difficult to gauge if Ti species are also incorporated into the nanoparticles, as discriminating TiO_x species from Ti in bulk $SrTiO_3$ constitutes a significant challenge. Presumably however, the encapsulation of a TiO_x species would lead to changes in the chemical state of platinum. Thus, it is reasonable that our annealing conditions brought about changes in the Pt nanoparticles to prevent complete coalescence, which would further indicate the promise that these Pt nanostructures have for applications with harsh environments such as heterogeneous catalysis.

5. Conclusions

We demonstrate the formation of Pt nanoparticles via evaporation and annealing in vacuum that exhibits a peculiar morphology that resists complete coalescence and reduction in surface area. From AFM and SEM, the platinum appears to form clusters of smaller nanoparticles that are 2–4 nm tall, 10–50 nm across, and spaced ~100 nm apart. GISAXS measurements support these nanoparticle dimensions quantitatively and also indicate the presence of nanoparticle clusters. Platinum hierarchical nanostructures such as these and the cluster deposited Pt structures [1–3] retain a high surface-to-volume ratio that is necessary for maximizing chemical activity for applications such as catalysis. These structures stand to significantly reduce the cost of using noble metal catalysts as a high surface-to-volume ratio combined with resistance to coalescence could yield longer catalyst service and efficiency.

Acknowledgements

The authors are grateful to P.W. Voorhees for useful discussions on nucleation and growth phenomena of materials on surfaces. This work was supported by the Institute for Catalysis in Energy Processes (U.S. Department of Energy Grant DE-FG02-03ER15457). Argonne National Laboratory (ANL) is a U.S. Department of Energy Office of Science Laboratory operated under Contract No. DE-AC02-06CH11357 by UChicago Argonne, LLC. X-ray measurements were performed at ANL's Advanced Photon Source, Sector 12 (BESSRC), and at Sector 5 (DND-CAT) which is also supported in part by: E.I. DuPont de Nemours & Co., Dow Chemical Co. and the State of Illinois. This work made use of Northwestern University Central Facilities supported by the MRSEC through NSF Contract No. DMR-0520513.

References

[1] R. Alayan, L. Arnaud, M. Broyer, E. Cottancin, J. Lerme, S. Marhaba, J.L. Vialle, M. Pellarin, Organization of size-selected platinum and indium clusters soft-landed on surfaces, Phys. Rev. B 76 (2007) 075424.
[2] D. Tainoff, L. Bardotti, F. Tournus, G. Guiraud, O. Boisron, P. Melinon, Self-organization of size-selected bare platinum nanoclusters: toward ultra-dense catalytic systems, J. Phys. Chem. C 112 (2008) 6842–6849.
[3] S. Stappert, B. Rellinghaus, M. Acet, E.F. Wassermann, Gas-phase preparation of L1(0) ordered FePt nanoparticles, J. Cryst. Growth 252 (2003) 440–450.
[4] F.T. Wagner, S. Ferrer, G.A. Somorjai, Photocatalytic hydrogen production from water over $SrTiO_3$ crystal surfaces, electron-spectroscopy studies of adsorbed H_2, O_2 and H_2O, Surf. Sci. 101 (1980) 462–474.
[5] F.T. Wagner, G.A. Somorjai, Photocatalytic and photoelectrochemical hydrogen production on strontium titanate single crystals, J. Am. Chem. Soc. 102 (1980) 5494–5502.
[6] R.G. Carr, G.A. Somorjai, Hydrogen production from photolysis of steam adsorbed onto platinized $SrTiO_3$, Nature 290 (1981) 576–577.
[7] G. Binnig, C.F. Quate, C. Gerber, Atomic force microscope, Phys. Rev. Lett. 56 (1986) 930–933.
[8] J.R. Levine, L.B. Cohen, Y.W. Chung, P. Georgopoulos, Grazing-incidence small-angle X-Ray scattering—new tool for studying thin-film growth, J. Appl. Crystallogr. 22 (1989) 528–532.
[9] M. Schmidbauer, T. Wiebach, H. Raidt, M. Hanke, R. Kohler, H. Wawra, Ordering of self-assembled $Si_{1-x}Ge_x$ islands studied by grazing incidence small-angle X-ray scattering and atomic force microscopy, Phys. Rev. B 58 (1998) 10523–10531.
[10] S.T. Christensen, J.W. Elam, B. Lee, Z. Feng, M.J. Bedzyk, M.C. Hersam, Nanoscale structure and morphology of atomic layer deposition platinum on $SrTiO_3$ (0 0 1), Chem. Mater. 21 (2009) 516.
[11] M. Kawasaki, K. Takahashi, T. Maeda, R. Tsuchiya, M. Shinohara, O. Ishiyama, T. Yonezawa, M. Yoshimoto, H. Koinuma, Atomic control of the $SrTiO_3$ crystal surface, Science 266 (1994) 1540–1542.
[12] G. Koster, G. Rijnders, D.H.A. Blank, H. Rogalla, Surface morphology determined by (0 0 1) single-crystal $SrTiO_3$ termination, Physica C 339 (2000) 215–230.
[13] M. Naito, H. Sato, Reflection high-energy electron diffraction study on the $SrTiO_3$ surface structure, Physica C 229 (1994) 1–11.
[14] R. Lazzari, IsGISAXS: a program for grazing-incidence small-angle X-ray scattering analysis of supported islands, J. Appl. Crystallogr. 35 (2002) 406–421.
[15] A. Guinier, G. Fournet, Small-angle Scattering of X-rays, John Wiley & Sons, New York, 1955.
[16] B. Lee, I. Park, J. Yoon, S. Park, J. Kim, K.W. Kim, T. Chang, M. Ree, Structural analysis of block copolymer thin films with grazing incidence small-angle X-ray scattering, Macromolecules 38 (2005) 4311–4323.
[17] M. Rauscher, T. Salditt, H. Spohn, Small-angle X-ray scattering under grazing incidence: the cross section in the distorted-wave Born approximation, Phys. Rev. B 52 (1995) 16855–16863.
[18] G. Renaud, R. Lazzari, C. Revenant, A. Barbier, M. Noblet, O. Ulrich, F. Leroy, J. Jupille, Y. Borensztein, C.R. Henry, J.P. Deville, F. Scheurer, J. Mane-Mane, O. Fruchart, Real-time monitoring of growing nanoparticles, Science 300 (2003) 1416–1419.

[19] B. Lee, S. Seifert, S.J. Riley, G. Tikhonov, N.A. Tomczyk, S. Vajda, R.E. Winans, Anomalous grazing incidence small-angle X-ray scattering studies of platinum nanoparticles formed by cluster deposition, J. Chem. Phys. 123 (2005) 074701.
[20] J.S. Pedersen, Determination of size distributions from small-angle scattering data for systems with effective hard-sphere interactions, J. Appl. Crystallogr. 27 (1994) 595–608.
[21] R. Hosemann, S.N. Bagchi, Direct Analysis of Matter by Diffraction, Amsterdam, North-Holland, 1962.
[22] M.R. Castell, Scanning tunneling microscopy of reconstructions on the $SrTiO_3$ (0 0 1) surface, Surf. Sci. 505 (2002) 1–13.
[23] O. Dulub, W. Hebenstreit, U. Diebold, Imaging cluster surfaces with atomic resolution: the strong metal-support interaction state of Pt supported on TiO_2 (1 1 0), Phys. Rev. Lett. 84 (2000) 3646–3649.
[24] Q. Fu, T. Wagner, Interaction of nanostructured metal overlayers with oxide surfaces, Surf. Sci. Rep. 62 (2007) 431–498.